Supporting Appendix

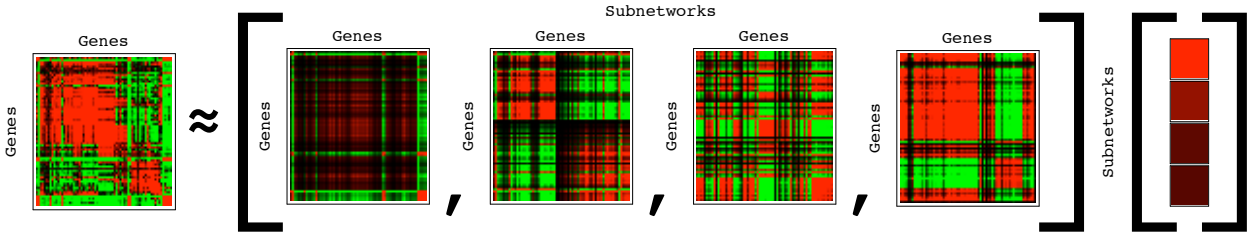

Fig. 5. The eigenvalue decomposition (EVD) [13] of the symmetric yeast network $\hat{a}_1$ of 4,153-genes × 4,153-genes correlations [4–6], computed from the genome-scale mRNA expression data signal $\hat{e}_1$ of 4,153-genes × 18-samples of a cell cycle time course of an α factor-synchronized culture [1] (Mathematica Notebook 1 and Data Set 1). Raster display of $\hat{a}_1 \approx \sum_{m=1}^{4} \epsilon_{1,m}^2 |\alpha_{1,m}\rangle\langle\alpha_{1,m}|$, with correlation (red), decorrelation (black), and anticorrelation (green) in expression, visualizing the network as an approximate superposition of only its four most significant EVD subnetworks, in the subset of 70 genes which constitute the 150 correlations in each subnetwork that are largest in amplitude among the 2,926 correlations of 77 traditionally-classified cell cycle-regulated genes [1] (Data Set 2). The subnetworks are associated with the functionally independent pathways that are manifest in the signal $\hat{e}_1$. The first and most significant subnetwork is associated with the α factor signal transduction pathway. The second subnetwork is associated with the exit from the α factor-induced cell cycle arrest in the cell cycle stage M/G_1 and the entry into the cell cycle stage G_1. The third and fourth subnetworks, which are of similar significance, are associated with the two pathways of antipodal cell cycle expression oscillations, which are orthogonal, i.e., $\pi/2$ out of phase relative to one another, at the cell cycle stage S vs. those at M, and at G_1 vs. G_2, respectively.

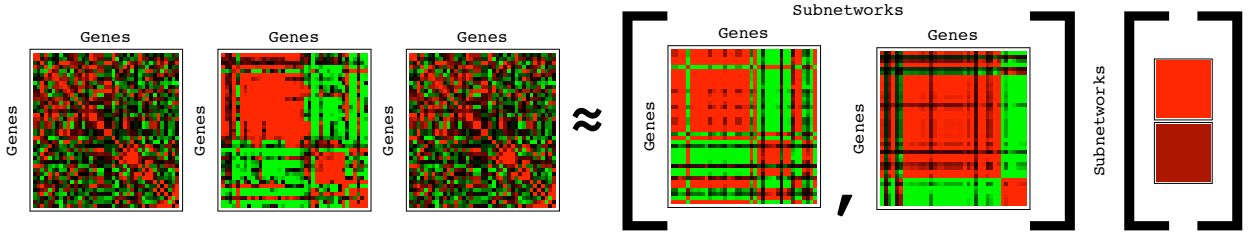

Fig. 6. The pseudoinverse projection [12, 13] of the network $\hat{a}_1$ onto a genome-scale proteins' DNA-binding basis signal of 2,120-genes × 12-samples of cell cycle transcription factors [3] (Mathematica Notebook 2 and Data Set 3), computed for the 1,588 genes at the intersection of $\hat{a}_1$ and the basis signal. Raster display of the pseudoinverse-projected network $\hat{a}_2 \equiv (\hat{b}\hat{b}^\dagger)\hat{a}_1(\hat{b}\hat{b}^\dagger) \approx \sum_{m=1}^{2} \epsilon_{2,m}^2 |\alpha_{2,m}\rangle\langle\alpha_{2,m}|$, visualizing this network as an approximate superposition of only its two most significant EVD subnetworks, in the subset of 39 genes which constitute the 200 correlations in each subnetwork that are largest in amplitude among the 1,128 correlations of 48 traditionally-classified cell cycle-regulated genes. The subnetworks are associated with the functionally independent pathways that are manifest in both the data and basis signals. The two most significant subnetworks are associated with the two pathways of antipodal cell cycle expression oscillations, which are orthogonal, i.e., $\pi/2$ out of phase relative to one another, at the cell cycle stage G_1 vs. those at G_2, and at S vs. M, respectively. The α factor signal transduction pathway and the transition from the α factor-induced cell cycle arrest into the cell cycle progression, that are manifest in the data but not in the basis signal, are not associated with either one of the significant subnetworks of $\hat{a}_2$.

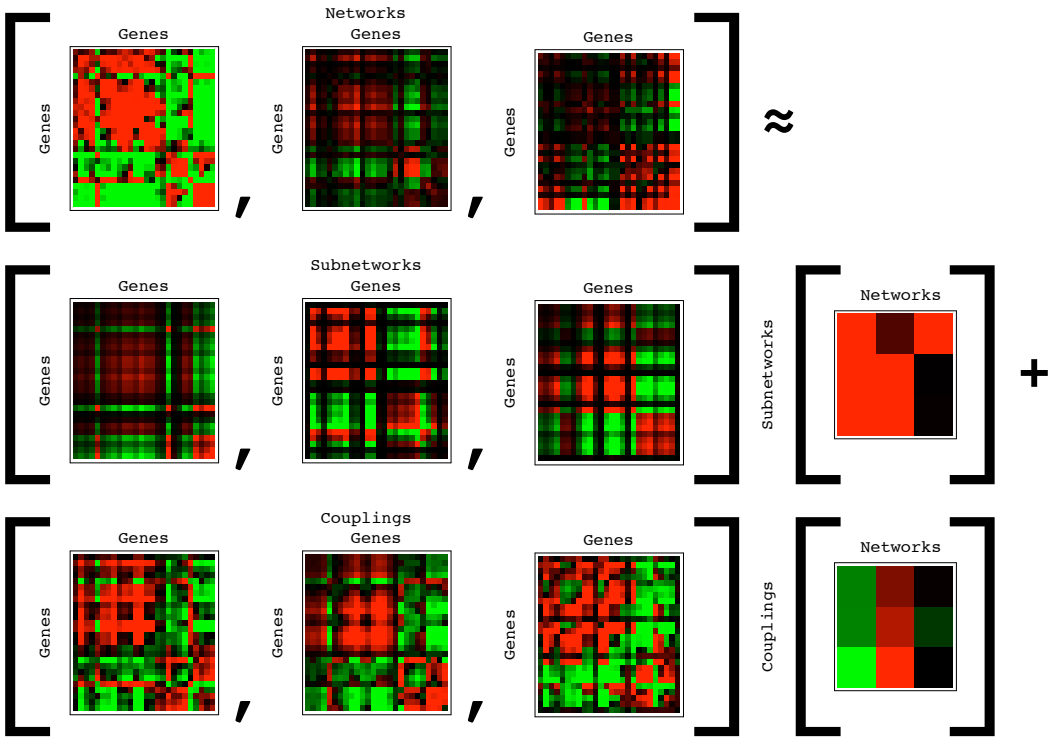

Fig. 7. A higher-order EVD (HOEVD) of the third-order series of the three networks $\{\hat{a}_1, \hat{a}_2, \hat{a}_3\}$. The network $\hat{a}_3$ is the pseudoinverse projection of the network $\hat{a}_1$ onto a genome-scale proteins' DNA-binding basis signal of 2,476-genes $\times$ 12-samples of development transcription factors [3] (Mathematica Notebook 3 and Data Set 4), computed for the 1,827 genes at the intersection of $\hat{a}_1$ and the basis signal. The HOEVD is computed for the 868 genes at the intersection of $\hat{a}_1$, $\hat{a}_2$ and $\hat{a}_3$. Raster display of $\hat{a}_k \approx \sum_{m=1}^{3} \epsilon_{k,m}^2 |\alpha_m\rangle\langle\alpha_m| + \sum_{m=1}^{3} \sum_{l=m+1}^{3} \epsilon_{k,lm}^2 (|\alpha_l\rangle\langle\alpha_m| + |\alpha_m\rangle\langle\alpha_l|)$, for all $k = 1, 2, 3$, visualizing each of the three networks as an approximate superposition of only the three most significant HOEVD subnetworks and the three couplings among them, in the subset of 26 genes which constitute the 100 correlations in each subnetwork and coupling that are largest in amplitude among the 435 correlations of 30 traditionally-classified cell cycle-regulated genes. This tensor HOEVD is different from the tensor higher-order SVD [14–16] for the series of symmetric nonnegative matrices $\{\hat{a}_1, \hat{a}_2, \hat{a}_3\}$. The subnetworks correlate with the genomic pathways that are manifest in the series of networks. The most significant subnetwork correlates with the response to the pheromone. This subnetwork does not contribute to the expression correlations of the cell cycle-projected network $\hat{a}_2$, where $\epsilon_{2,1}^2 \approx 0$. The second and third subnetworks correlate with the two pathways of antipodal cell cycle expression oscillations, at the cell cycle stage G_1 vs. those at G_2, and at S vs. M, respectively. These subnetworks do not contribute to the expression correlations of the development-projected network $\hat{a}_3$, where $\epsilon_{3,2}^2 \approx \epsilon_{3,3}^2 \approx 0$. The couplings correlate with the transitions among these independent pathways that are manifest in the individual networks only. The coupling between the first and second subnetworks is associated with the transition between the two pathways of response to pheromone and cell cycle expression oscillations at G_1 vs. those G_2, i.e., the exit from pheromone-induced arrest and entry into cell cycle progression. The coupling between the first and third subnetworks is associated with the transition between the response to pheromone and cell cycle expression oscillations at S vs. those at M, i.e., cell cycle expression oscillations at G_1/S vs. those at M. The coupling between the second and third subnetworks is associated with the transition between the orthogonal cell cycle expression oscillations at G_1 vs. those at G_2 and at S vs. M, i.e., cell cycle expression oscillations at the two antipodal cell cycle checkpoints of G_1/S vs. G_2/M. All these couplings add to the expression correlation of the cell cycle-projected $\hat{a}_2$, where $\epsilon_{2,12}^2, \epsilon_{2,13}^2, \epsilon_{2,23}^2 > 0$; their contributions to the expression correlations of $\hat{a}_1$ and the development-projected $\hat{a}_3$ are negligible (see also Fig. 4).

Significant EVD Subnetworks are Associated with Functionally Independent Pathways. The data signal $\hat{e}_1$ we analyze tabulates relative mRNA expression levels of $N = 4,153$ yeast genes with valid data in at least 15 of the $M_1 = 18$ samples of a cell cycle time course of an α factor-synchronized culture monitored by Spellman et al. [1]. The relative expression level of the nth gene in the mth sample is presumed valid when the

ratio of the measured expression to the background signal is > 1.5 for both the synchronized culture and asynchronous reference (Data Set 1). We use SVD to estimate these missing data [10] (and see also [18]) and to approximately center the expression pattern of each gene at its sample-, i.e. time-invariant level [9] (Mathematica Notebook 1).

For the nth gene $|g_{1,n}\rangle$ with missing data in $M_1' < M_1$ of the arrays, we estimate the missing expression level in the mth array $\langle m|g_{1,n}\rangle$ to be a superposition of the $L' < M_1 - M_1'$ significant eigengenes $\{|\gamma_{1,l}'\rangle\}$ in the mth array as computed for the subset of $N' < N$ genes with no missing data in any of the M_1 arrays. The coefficients of this superposition are determined by the expansion of the expression of the nth gene across all $M_1 - M_1'$ arrays with no missing data, $|g_{1,n}\rangle_{M_1'}$, in the subspace spanned by the significant eigengenes across the same $M_1 - M_1'$ arrays, $\{|\gamma_{1,l}'\rangle_{M_1'}\}$, such that $\langle m|g_{1,n}\rangle \rightarrow \sum_{l=1}^{L'} \langle m|\gamma_{1,l}'\rangle\ {}_{M_1'}\langle\beta_{1,l}'|g_{1,n}\rangle_{M_1'}$, where $\{\ {}_{M_1'}\langle\beta_{1,l}'|\}$ span the $L' \times (M - M_1')$ subspace $(\hat{v}_{M_1'}')^\dagger$ that is pseudoinverse to the $(M - M_1') \times L'$ subspace $\hat{v}_{M_1'}'$, which is spanned by $\{|\gamma_{1,l}'\rangle_{M_1'}\}$.

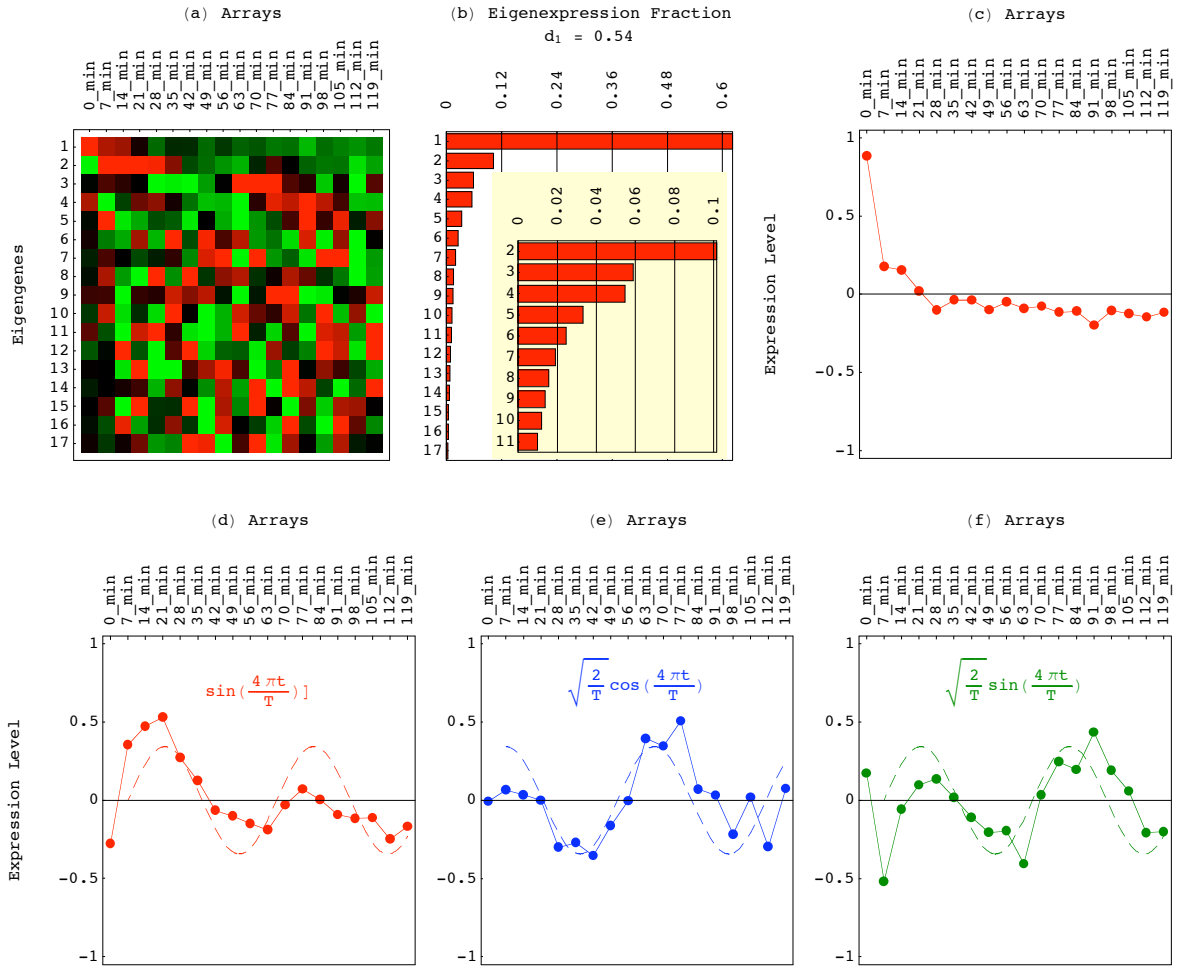

Fig. 8. Eigengenes of the data signal $\hat{e}_1$ as computed for the 4,153 genes after missing data estimation and approximate centering. (*a*) Raster display. (*b*) Bar chart of the fractions of eigenexpressions. (*c–f*) Line-joined graphs of the first (red), second (red), third (blue) and fourth (green) eigengenes, respectively, describe expression patterns across the arrays that are consistent with the associations of the corresponding subnetworks. The first eigengene describes an initial transient increase in expression superimposed on time-invariant expression (as well as the antiparallel pattern of initial decrease in expression). The second eigengene describes an initial transient increase superimposed on periodic expression oscillations that fit a dashed graph of a normalized sine of two periods (red). The third and fourth eigengenes describe periodic expression oscillations that fit dashed graphs of normalized cosine (blue) and sine (green) functions, respectively, of two periods.

We use the 5 most significant eigengenes as computed for the subset of 2,493 genes with no missing data in the 18 arrays in order to estimate the missing data in the remaining 1,660 genes. We find that these eigenegenes and corresponding fractions of eigenexpression are similar to those computed for the full set of 4,153 genes after the missing data are estimated suggesting that the five most significant eigengenes, as computed for the 2,493 genes with no missing data, are meaningful patterns for estimating the missing data in the data signal. This also illustrates the robustness of the significant SVD eigenexpression levels as well as eigengenes to perturbations in the genes that compose the data signal $\hat{e}_1$.

After missing data estimation the first eigengene, which captures ≈90% of the expression information and describes expression that is approximately invariant across the samples, i.e., in time, is inferred to represent steady-state expression. We filter out this eigengene and the corresponding eigenarray without eliminating genes or arrays from the data signal by setting the corresponding eigenexpression level in $\hat{\epsilon}_1$ to zero and reconstructing the data signal from $\hat{u}_1\hat{\epsilon}_1\hat{v}_1^T$. After filtering out the first eigengene, the expression pattern of each gene is approximately centered at its sample-, i.e. time-invariant level (Fig. 8).

Classification	Eigenarray	Most likely parallel association	P value of parallel association	Most likely antiparallel association	P value of antiparallel association
Cell Cycle	1	M/G_1	9.3×10^{-10}	G_1	7.8×10^{-18}
	2	G_1	3.4×10^{-55}	G_2/M	8.2×10^{-30}
	3	M/G_1	3.9×10^{-39}	S/G_2	1.9×10^{-23}
	4	G_1	1.1×10^{-69}	G_2/M	1.5×10^{-33}
Pheromone Response	1	Up	3.4×10^{-65}	Down	5.7×10^{-54}
	2	Down	4.3×10^{-12}	Up	1.5×10^{-16}
	3	Down	5.4×10^{-9}	Down	8.9×10^{-14}
	4	Down	5.6×10^{-29}	Down	4.2×10^{-5}

Table 1. Most likely parallel and antiparallel associations of the significant SVD eigenarrays of the data signal $\hat{e}_1$ according to the traditional and microarray classifications of cell cycle-regulated [1] and pheromone-regulated [2] yeast genes, are consistent with the associations of the corresponding subnetworks.

Classification	Subnetwork	Most likely parallel association	P value of parallel association	Most likely antiparallel association	P value of antiparallel association
Cell Cycle	1	S S	1.7×10^{-22}	M/G_1 S	5.1×10^{-7}
	2	G_1 G_1	1.3×10^{-29}	G_1 G_2/M	3.2×10^{-11}
	3	S S	2.1×10^{-30}	M/G_1 S	2.6×10^{-25}
	4	G_1 S	2.1×10^{-28}	G_1 G_2/M	5.7×10^{-24}
Pheromone Response	1	Up Up	4.0×10^{-53}	Down Up	2.2×10^{-50}
	2	Down Down	1.6×10^{-11}	Down Up	9.8×10^{-17}
	3	Down Down	6.2×10^{-6}	Down Down	1.6×10^{-11}
	4	Down Down	8.0×10^{-32}	Down Down	2.5×10^{-6}

Table 2. Most likely parallel and antiparallel associations of the significant EVD subnetworks of the network $\hat{a}_1$ according to the traditional and microarray classifications of cell cycle- and pheromone-regulated yeast genes.

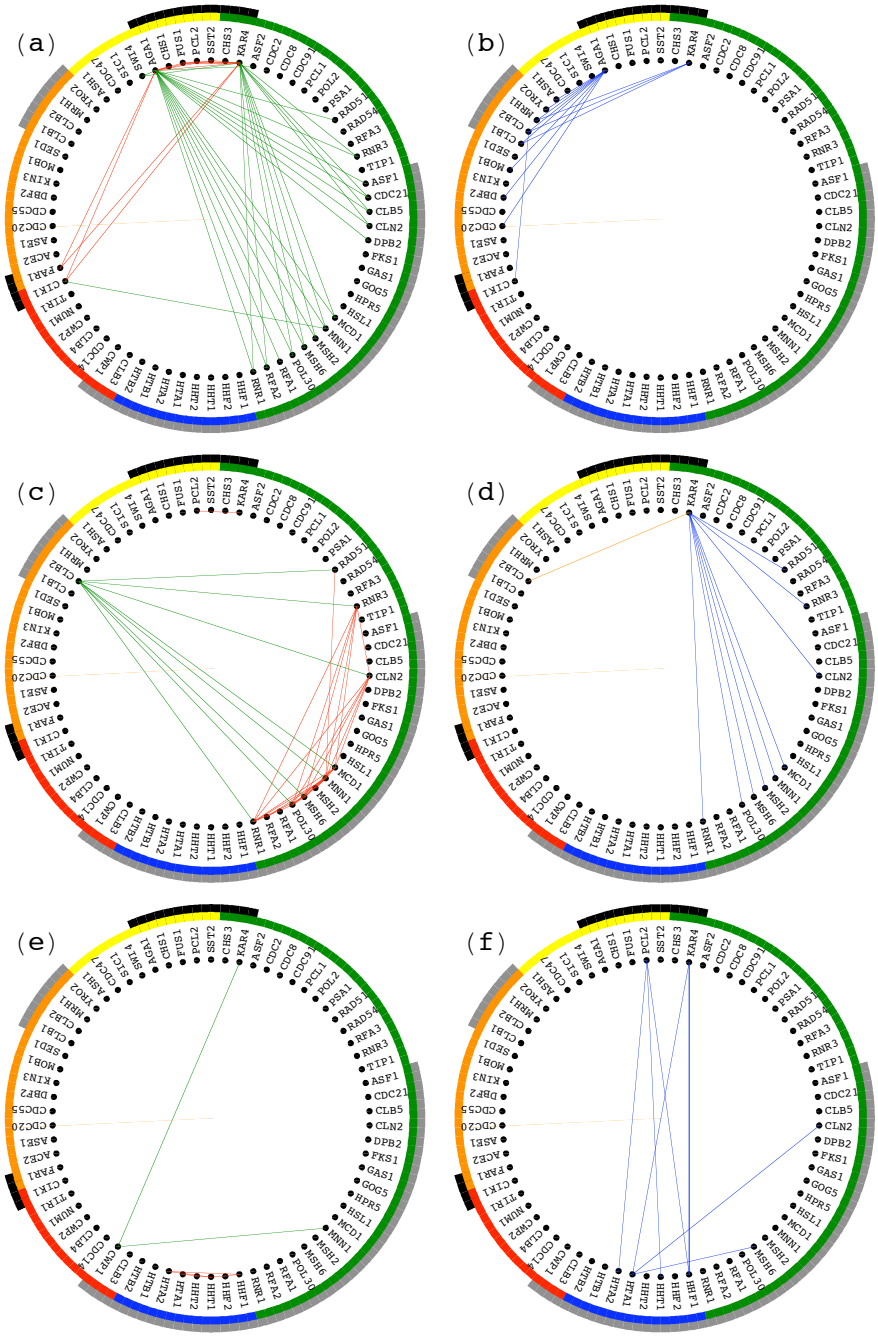

Fig. 9. Boolean functions of the discretized significant EVD subnetworks [6] of the network $\hat{a}_1$ in the subsets of 150 relations largest in amplitude among all traditionally-classified cell cycle genes of $\hat{a}_1$, color-coded according to their cell cycle classifications, M/G_1 (yellow), G_1 (green), S (blue), S/G_2 (red) and G_2/M (orange), and separately also their pheromone response classifications, up-regulated (black) and down-regulated (gray). (*a*) Intersection of the first AND second subnetworks of $\hat{a}_1$ highlights pheromone response-dependent correlations (red), such as that between *KAR4* and *CIK1* [8], as well as anticorrelations (green), such as that between *KAR4* and *CLN2*. (*b*) Intersection of the first AND NOT second subnetworks of $\hat{a}_1$ highlights relations (blue) among genes that are antipodal in the pathway of pheromone signal transduction vs. the pathway of exit from pheromone-induced arrest and entry into cell cycle progression. Highighted relations correspond to anticorrelations in the first subnetwork and correlations in the second subnetwork. For example, *AGA1* and *CLB2* are anticorrelated in the pheromone signal transduction pathway but are correlated in the pathway of entry into cell cycle progression at the cell cycle stage G_1. Also included are the relations between the pheromone-response up-regulated *KAR4*, which cell cycle expression peaks at G_1 and pheromone-response down-regulated *CLB1* and *CLB2*, which cell cycle expression peaks at G_2/M. (*c*) Intersection of the second

AND fourth subnetworks highlights correlations (red) among G_1 genes and their anticorrelations (green) with *CLB2* that encodes a G_2/M cyclin. (*d*) Intersection of the second AND NOT fourth subnetworks highlights correlations in the second subnetwork that correspond to anticorrelations in the fourth (orange) and anticorrelations in the second that correspond to correlations in the fourth (blue). All relations that are antipodal in the pathway of exit from pheromone-induced arrest and entry into G_1 vs. that of cell cycle expression oscillations at G_1 vs. G_2, are between the pheromone-response up-regulated *KAR4* and down-regulated genes. *KAR4* and *CLN2*, for example, are anticorrelated during the exit from the pheromone-induced arrest but correlated during the cell cycle stage G_1. Similarly, *KAR4* and *CLB2* are correlated during the exit from the pheromone-induced arrest but anticorrelated during G_1. (*e*) Intersection of the third AND fourth subnetworks shows very few relations that are common to the two orthogonal pathways of antipodal cell cycle expression oscillations, at S vs. M, and at G_1 vs. G_2, respectively. These common relations include correlations (red) among S genes and an anticorrelation (green) between *MNN1* and *CWP1*, which encode glycoproteins that are active at the antipodal stages G_1 and S/G_2, respectively [19]. (*f*) Intersection of the third AND NOT fourth subnetworks shows very few anticorrelations in the third subnetwork that correspond to correlations in the fourth (blue). All relations that are antipodal in the pathway of cell cycle expression oscillations at G_1 vs. G_2 vs. the pathway of oscillations at S vs. M are between G_1 and M/G_1 genes, such as *CLN2*, and S stage histones.

Integrative Pseudoinverse-Projected Networks Simulate Observation of Only the Pathways Manifest in Both the Data and Basis Signals. The basis signals we analyze tabulate relative DNA-bound occupancy levels of (i) 2,120 genes in $L = 12$ samples of the 12 cell cycle transcription factors Ace2, Fkh1, Fkh2, Mbp1, Mcm1, Ndd1, Rme1, Skn7, Stb, Swi4, Swi5 and Swi6 (Data Set 3); (ii) 2,476 genes in 12 samples of the development transcription factors Ash1, Dig1, Hms1, Ime4, MATa1, Mot3, Phd1, Rim101, Rlm1, Sok2, Ste12 and Sum1 (Data Set 4); and (iii) 2,943 genes in eight samples of the biosynthesis factors Abf1, Dot6, Fhl1, Hir1, Hir2, Rap1, Reb1 and Rgm1 (Data Set 5) measured by Lee et al. [3]. We use SVD to approximately center the pattern of binding of each gene [9] (Mathematica Notebook 2).

The most significant eigengene of each one of the basis signals is approximately invariant across the samples, and is inferred to represent steady-state binding. We filter out these eigengenes and the corresponding eigenarrays without eliminating genes or arrays from either basis signal by setting the corresponding eigenbinding level in the SVD of each basis signal to zero. After filtering out the first eigengene, the binding pattern of each gene is approximately centered at its sample-, i.e. transcription factor-invariant level.

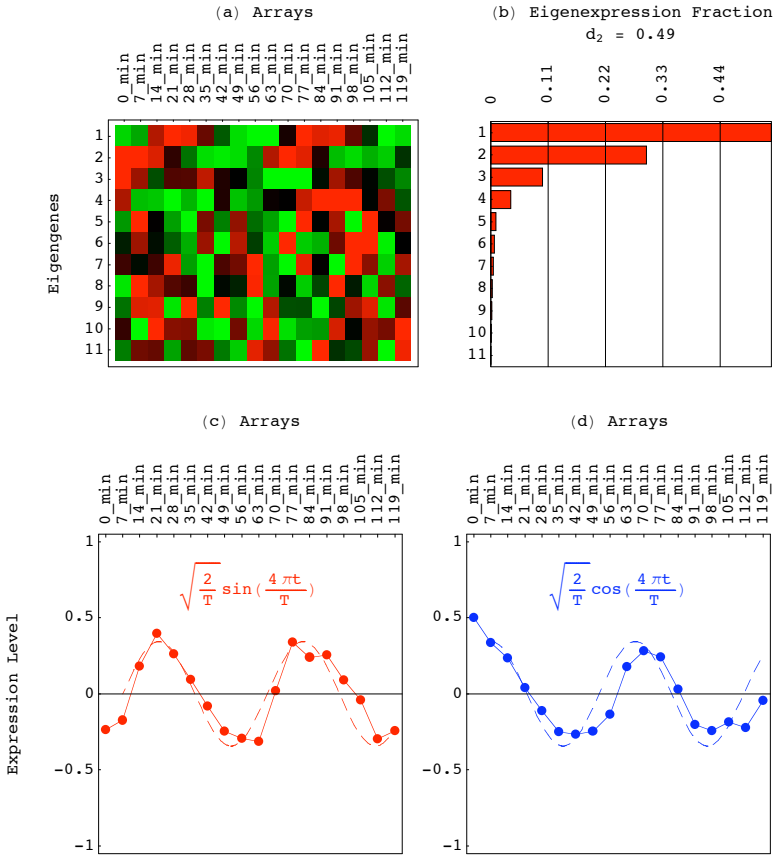

Fig. 10. Eigengenes of $\hat{e}_2$, i.e., the data signal $\hat{e}_1$ pseudoinverse-projected onto the cell cycle transcription factors' DNA-binding basis signal. (*a*) Raster display. (*b*) Bar chart of the fractions of eigenexpressions. (*c* and *d*) Line-joined graphs of the first (red) and second (blue) eigengenes fit dashed graphs of normalized sine (red) and cosine (blue) functions, respectively, of two periods, and are consistent with the associations of the corresponding subnetworks with the two orthogonal pathways of cell cycle expression oscillations.

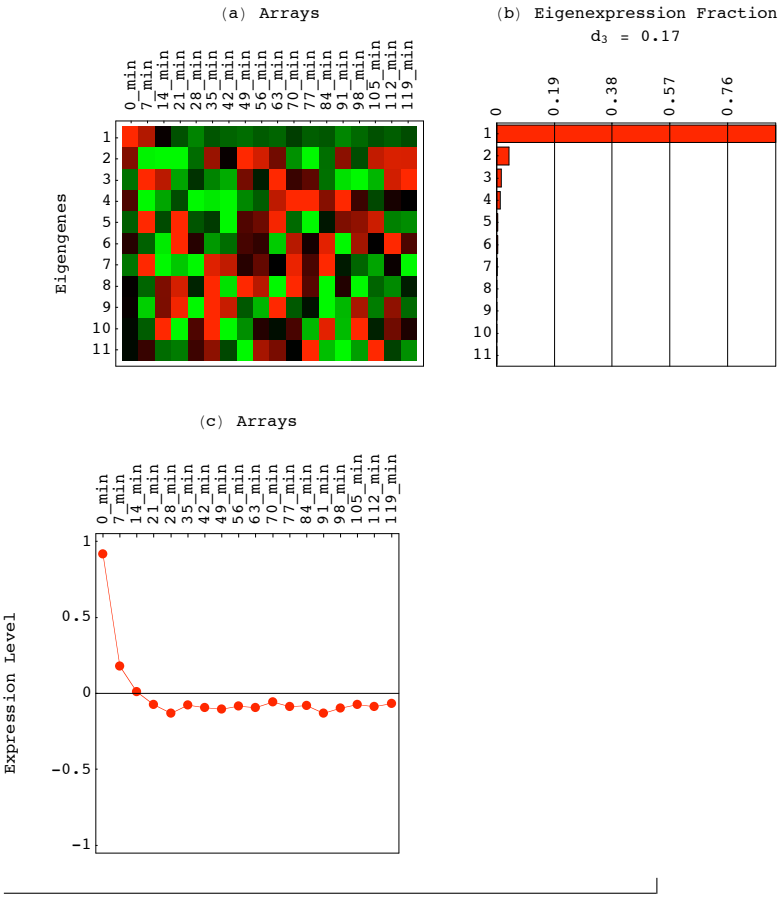

Fig. 11 (*left*). Eigengenes of $\hat{e}_3$, i.e., $\hat{e}_1$ pseudoinverse-projected onto the development basis signal. (*a*) Raster display. (*b*) Bar chart of the fractions of eigenexpressions. (*c*) Line-joined graph of the first (red) eigengene describes an initial transient increase in expression superimposed on time-invariant expression, and is consistent with the association of the corresponding subnetwork with the pheromone signal transduction pathway.

Fig. 12 (*below*). Eigengenes of $\hat{e}_4$, i.e., $\hat{e}_1$ pseudoinverse-projected onto the biosynthesis basis signal. (*a*) Raster display. (*b*) Bar chart of the fractions of eigenexpressions. (*c–e*) Line-joined graphs of the first (red), second (blue) and third (green) eigengenes fit dashed graphs of normalized sine (red) and cosine (blue, green) functions, respectively, of two periods, and are consistent with the associations of the corresponding subnetworks with the expression of histones during DNA replication at the cell cycle stage S.

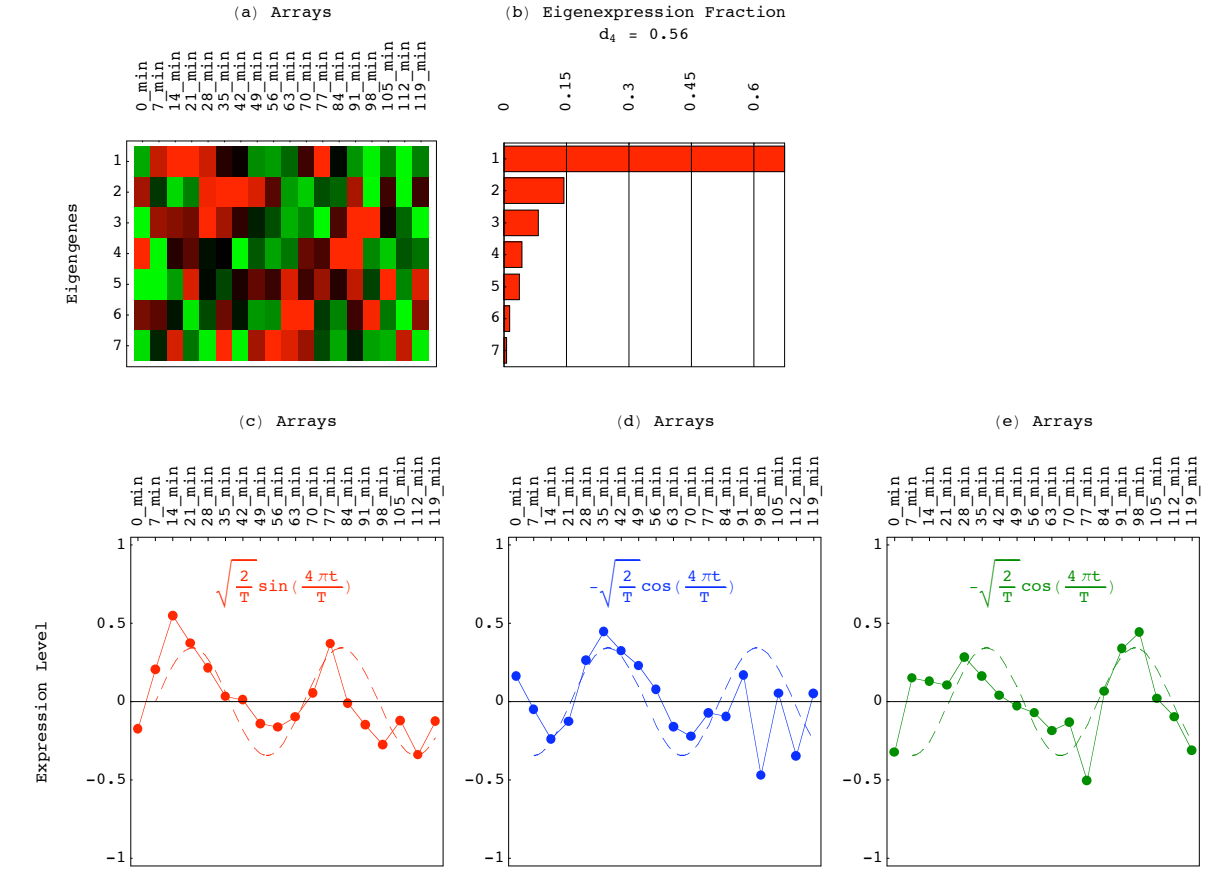

		Classification	Eigenarray	Most likely parallel association	P value of parallel association	Most likely antiparallel association	P value of antiparallel association
a	Cell Cycle	Cell Cycle	1	G_1	9.4×10^{-19}	G_2/M	1.4×10^{-15}
			2	M/G_1	2.2×10^{-12}	G_2/M	1.5×10^{-7}
		Pheromone	1	Down	1.0×10^{-14}	Up	2.3×10^{-1}
			2	Up	2.3×10^{-4}	Down	1.7×10^{-17}
b	Development	Cell Cycle	1	M/G_1	6.9×10^{-3}	None	9.8×10^{-2}
		Pheromone	1	Up	1.0×10^{-10}	None	2.9×10^{-3}
c	Biosynthesis	Cell Cycle	1	G_1	9.0×10^{-8}	None	1.9×10^{-3}
			2	S	5.3×10^{-4}	None	2.1×10^{-2}
			3	G_2/M	1.9×10^{-5}	G_1	3.0×10^{-2}
		Pheromone	1	Down	2.6×10^{-1}	None	1.2×10^{-1}
			2	Down	7.6×10^{-2}	None	7.6×10^{-3}
			3	Down	6.3×10^{-5}	Down	7.6×10^{-2}

Table 3. Most likely parallel and antiparallel associations of the significant SVD eigenarrays of the pesudoinverse-projected signals $\hat{e}_2$, $\hat{e}_3$ and $\hat{e}_4$, i.e., $\hat{e}_1$ pseudoinverse-projected onto the (a) cell cycle, (b) development and (c) biosynthesis basis signals, according to the traditional and microarray classifications of cell cycle- and pheromone-regulated yeast genes.

	Transcription Factors	Classification	Subnetwork	Most likely parallel association	P value of parallel association	Most likely antiparallel association	P value of antiparallel association
a	Cell Cycle	Cell Cycle	1	G_1 G_1	1.3×10^{-9}	G_1 G_2/M	3.7×10^{-23}
			2	M/G_1 M/G_1	4.8×10^{-12}	G_2/M M/G_1	3.3×10^{-14}
		Pheromone	1	Down Down	6.8×10^{-5}	Down None	4.3×10^{-2}
			2	Up Up	2.5×10^{-5}	Down Up	1.6×10^{-15}
b	Development	Cell Cycle	1	M/G_1 M/G_1	1.8×10^{-9}	G_1 M/G_1	2.8×10^{-7}
		Pheromone	1	Up Up	1.8×10^{-23}	Down Up	2.5×10^{-17}
c	Biosynthesis	Cell Cycle	1	G_1 S/G_2	2.6×10^{-4}	S S/G_2	4.0×10^{-11}
			2	S S	2.8×10^{-24}	M/G_1 S	4.0×10^{-7}
			3	S S	1.1×10^{-26}	G_1 S	1.6×10^{-17}
		Pheromone	1	Down Down	4.6×10^{-3}	Down Down	7.6×10^{-2}
			2	Down Down	5.1×10^{-11}	Down Up	5.9×10^{-7}
			3	Down Down	4.0×10^{-23}	Down Down	9.0×10^{-10}

Table 4. Most likely parallel and antiparallel associations of the significant EVD subnetworks of the pseudoinverse-projected networks $\hat{a}_2$, $\hat{a}_3$ and $\hat{a}_4$, i.e., $\hat{a}_1$ pseudoinverse-projected onto the (a) cell cycle, (b) development and (c) biosynthesis basis signals, according to the traditional and microarray classifications of cell cycle- and pheromone-regulated yeast genes.

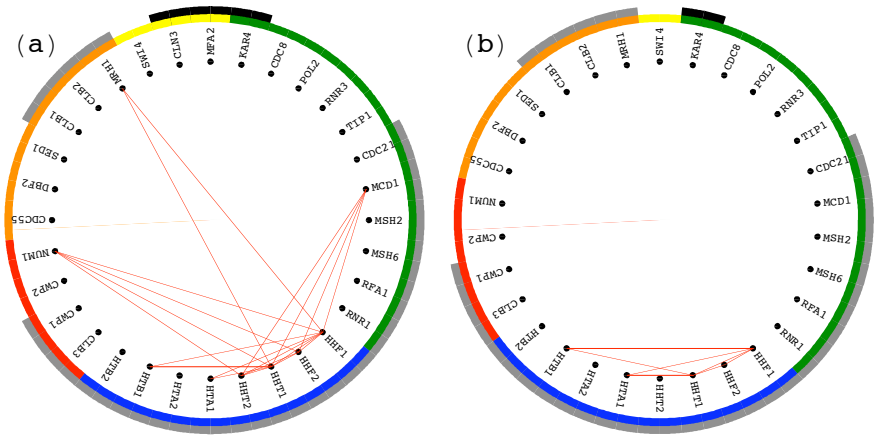

Fig. 13. Boolean functions of the discretized significant EVD subnetworks of the pseudoinverse-projected network $\hat{a}_4$ in the subsets of 200 relations largest in amplitude among all traditionally-classified cell cycle genes of $\hat{a}_4$, also with the third subnetwork of $\hat{a}_1$. (a) Intersection of the first AND second AND third subnetworks of $\hat{a}_4$ highlights correlations among the histones and other genes that are involved in biosynthesis of nuclear components, such as *MCD1* that is involved in sister chromatid cohesion. (b) Intersection of the first AND second AND third subnetworks of $\hat{a}_4$ AND the third subnetwork of $\hat{a}_1$, which is associated with expression at S vs. M, highlights correlations among histones.

Comparative HOEVD Subnetworks and Their Couplings are Associated with Pathways and the Transitions Among Them Common to the Series or Exclusive to a Subset of the Networks.

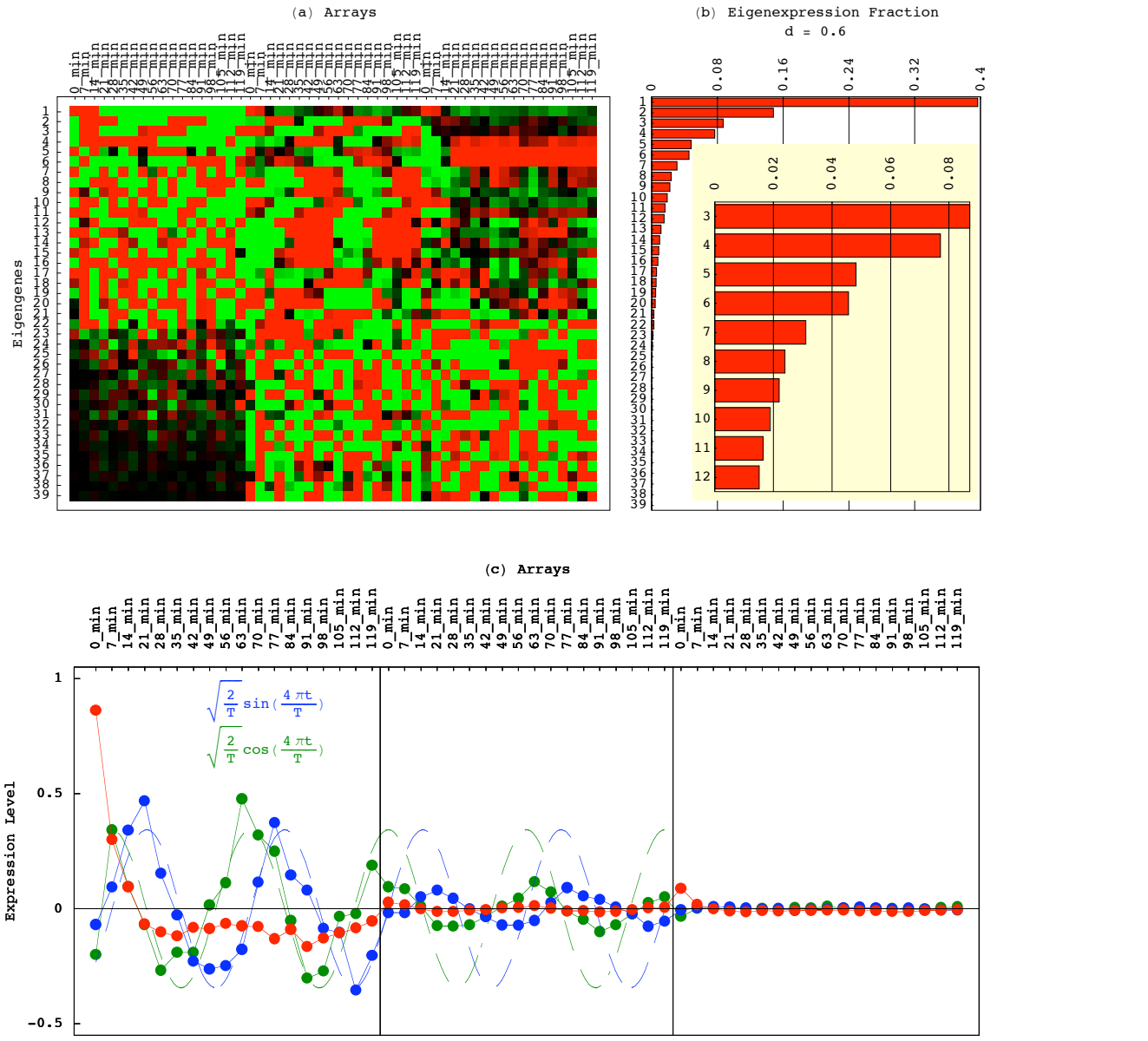

Fig. 14. Eigengenes of the appended signals $\hat{e} \equiv (\hat{e}_1, \hat{e}_2, \hat{e}_3)$ computed for the 868 genes at the intersection of $\hat{e}_1$, $\hat{e}_2$ and $\hat{e}_3$. (*a*) Raster display. (*b*) Bar chart of the fractions of eigenexpressions. (*c*) Line-joined graphs of the first (red), second (blue) and third (green) eigengenes, respectively, describe expression patterns across the arrays that are consistent with the associations of the corresponding subnetworks and their couplings with the independent pathways that are manifest in the overall network as well as the individual networks, and the transitions among these independent pathways that are manifest in the individual networks only. The first eigengene describes an initial transient increase in expression superimposed on time-invariant expression. The second and third eigengenes describe periodic expression oscillations that fit dashed graphs of normalized sine (blue) and cosine (green) functions, respectively, of two periods.

Classification	Eigenarray	Most likely parallel association	P value of parallel association	Most likely antiparallel association	P value of antiparallel association
Cell Cycle	1	M/G_1	8.0×10^{-7}	G_1	8.3×10^{-20}
	2	G_1	1.4×10^{-36}	G_2/M	5.5×10^{-18}
	3	M/G_1	3.1×10^{-16}	G_1	4.8×10^{-12}
Pheromone Response	1	Up	5.3×10^{-18}	Down	5.5×10^{-23}
	2	Down	8.0×10^{-4}	Down	2.7×10^{-3}
	3	Up	1.8×10^{-3}	Down	1.6×10^{-9}

Table 5. Most likely parallel and antiparallel associations of the significant SVD eigenarrays of the appended signals $\hat{e} \equiv (\hat{e}_1, \hat{e}_2, \hat{e}_3)$ according to the traditional and microarray classifications of cell cycle- and pheromone-regulated yeast genes.

	Classification	Subnetwork or Coupling Between Subnetworks	Most likely parallel association	P value of parallel association	Most likely antiparallel association	P value of antiparallel association
a	Cell Cycle	1	M/G_1 M/G_1	2.2×10^{-5}	M/G_1 S	3.1×10^{-5}
		2	G_1 G_1	1.8×10^{-7}	G_1 G_2/M	2.4×10^{-8}
		3	G_1 S	1.4×10^{-6}	M/G_1 S	1.2×10^{-7}
	Pheromone Response	1	Down Down	7.5×10^{-16}	Down Up	2.0×10^{-27}
		2	Down None	1.6×10^{-2}	Down Up	2.6×10^{-2}
		3	Down Down	1.4×10^{-2}	Down Up	2.1×10^{-6}
b	Cell Cycle	$1 \leftrightarrow 2$	G_1 G_1	1.8×10^{-5}	G_1 M/G_1	6.2×10^{-9}
		$1 \leftrightarrow 3$	G_1 S	1.4×10^{-6}	M/G_1 S	1.2×10^{-7}
		$2 \leftrightarrow 3$	G_1 S	1.1×10^{-5}	G_1 G_2/M	1.6×10^{-7}
	Pheromone Response	$1 \leftrightarrow 2$	Down Down	2.3×10^{-10}	Down Up	2.7×10^{-10}
		$1 \leftrightarrow 3$	Down Down	1.1×10^{-7}	Down Up	3.6×10^{-14}
		$2 \leftrightarrow 3$	Down Down	1.6×10^{-8}	Down Up	3.9×10^{-5}

Table 6. Most likely parallel and antiparallel associations of the significant HOEVD subnetworks of the series of the three networks $\{\hat{a}_1, \hat{a}_2, \hat{a}_3\}$ and their couplings, according to the traditional and microarray classifications of cell cycle- and pheromone-regulated yeast genes.

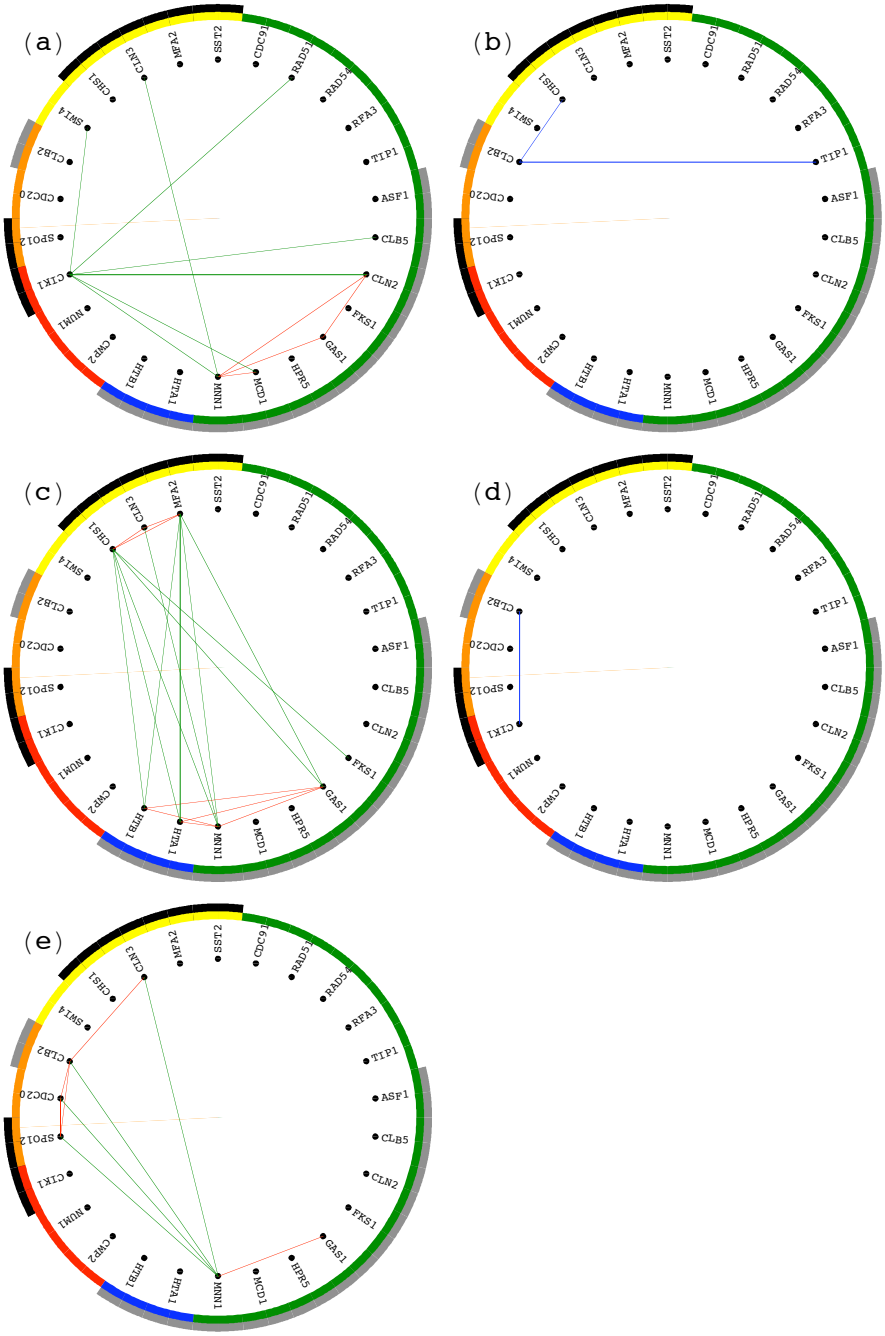

Fig. 15. Boolean functions of the discretized significant HOEVD subnetworks of the series of the three networks $\{\hat{a}_1, \hat{a}_2, \hat{a}_3\}$ and their couplings in the subsets of 100 relations largest in amplitude among all traditionally-classified cell cycle genes of the series highlight known as well as previously unknown pathway-dependent relations that are in agreement with current understanding of the cellular system of yeast. For example, *TIP1* that encodes a G_1 glycoprotein [19] is not reported to be regulated by pheromone. Yet, the correlation between *KAR4* and *TIP1* is common to all subnetworks and couplings, and is not limited to those that represent cell cycle pathways (see also Figs. 1–3). Our analyses, therefore, predict that *TIP1* is up-regulated in response to pheromone under the experimental conditions of Spellman et al. [1] (see also [2]), and that, e.g., the relation of *TIP1* with *CIK1* would follow the same pathway-depndence as that of *KAR4* with *CIK1*. The glycoproteins encoding *CWP1* and *MNN1* are classified as pheromone-regulated, suggesting further that additional cell cycle regulated glycoproteins might also be regulated by pheromone. (*a*) Intersection of the first AND second subnetworks AND the coupling between them highlights correlations among G_1 genes (red) and their anticorrelations (green) with S/G_2, G_2/M and M/G_1 genes. (*b*) Intersection of the first AND second subnetworks AND NOT the coupling between them highlights a couple of

relations (blue) among genes that correspond to anticorrelations in the pathway of pheromone signal transduction as well as the pathway of cell cycle expression oscillations at G_1 vs. those at G_2, but correspond to correlations in the transition between these two pathways, i.e., the exit from pheromone-induced arrest and entry into cell cycle progression at the cell cycle stage G_1. For example, *CLB2* and *TIP1* are classified into the antipodal cell cycle stages of G_2/M and G_1, respectively. While *CLB2* is classified as pheromone-response down-regulated, *TIP1* appears to be up-regulated in response to pheromone. These are consistent with their anticorrelations in the two pathways that the first and second subnetworks represent. During the transition between these two pathways, from pheromone-induced arrest to cell cycle progression, expression of both *CLB2* and *TIP1* is suppressed and therefore they are correlated in the transition between the pathways that the coupling between the first and second subnetworks represents. (*c*) Intersection of the first AND third subnetworks AND the coupling between them highlights correlations among G_1 and S genes, and also separately among M/G_1 genes (red) and anticorrelations among these two subsets of genes (green). (*d*) Intersection of the first AND third subnetworks AND NOT the coupling between them highlights a single relation (blue) among *CLB2* and *CIK1* that corresponds to an anticorrelation in the pathway of pheromone signal transduction as well as the pathway of cell cycle expression oscillations at S vs. those at M, but corresponds to a correlation in the transition between these two pathways, i.e., the exit from pheromone-induced arrest and entry into cell cycle progression at the cell cycle stage G_1/S. While *CLB2* is down-regulated by pheromone, *CIK1* is up-regulated. While *CLB2* encodes a G_2/M cyclin, *CIK1* peaks in expression at the stage S/G_2. These are consistent with their anticorrelations in the two pathways that the first and third subnetworks represent. During the transition between these two pathways, from pheromone-induced arrest to cell cycle progression, expression of both *CLB2* and *CIK1* is suppressed and therefore they are correlated in the transition between the pathways that the coupling between the first and third subnetworks represents. (*e*) Intersection of the second AND third subnetworks AND the coupling between them highlights correlations among G_2/M and M/G_1 genes (red) and their anticorrelations with *MNN1* that encodes a G_1 glycoprotein (green).

[1] Spellman, P. T., Sherlock, G., Zhang, M. Q., Iyer, V. R., Anders, K., Eisen, M. B., Brown, P. O., Botstein, D. & Futcher, B. (1998) *Mol. Biol. Cell* **9**, 3273–3297.

[2] Roberts, C. J., Nelson, B., Marton, M. J., Stoughton, R., Meyer, M. R., Bennett, H. A., He, Y. D., Dai, H., Walker, W. L., Hughes, T. R., Tyers, M., Boone, C., & Friend, S. H. (2000) *Science* **287**, 873–880.

[3] Lee, T. I., Rinaldi, N. J., Robert, F., Odom, D. T., Bar-Joseph, Z., Gerber, G. K., Hannett, N. M., Harbison, C. T., Thompson, C. M., Simon, I., Zeitlinger, J., Jennings, E. G., Murray, H. L., Gordon, D. B., Ren, B., Wyrick, J. J., Tagne, J. B., Volkert, T. L., Fraenkel, E., Gifford, D. K. & Young, R. A. (2002) *Science* **298**, 799–804.

[4] Ihmels, J., Levy, R. & Barkai, N. (2002) *Nat. Biotechnol.* **22**, 86–92.

[5] Balazsi, G., Barabasi, A. L. & Oltvai, Z. N. (2005) *Proc. Natl. Acad. Sci. USA* **102**, 7841–7846.

[6] Bowers, P. M., Cokus, S. J., Eisenberg, D. & Yeates, T. O. (2004) *Science* **306**, 2246–2249.

[7] Braun, E. & Brenner, N. (2004) *Phys. Biol.* **1**, 67–76.

[8] Kurihara, L. J., Stewart, B. G., Gammie, A. E. & Rose, M. D. (1996) *Mol. Cell. Biol.* **16**, 3990.

[9] Alter, O., Brown, P. O. & Botstein, D. (2000) *Proc. Natl. Acad. Sci. USA* **97**, 10101–10106.

[10] Alter, O., Brown, P. O. & Botstein, D. (2001) in *Microarrays: Optical Technologies and Informatics*, eds. Bittner, M. L., Chen, Y., Dorsel, A. N. & Dougherty, E. R. (Int. Soc. Optical Eng., Bellingham, WA) Vol. 4266, pp. 171–186.

[11] Alter, O., Brown, P. O. & Botstein, D. (2003) *Proc. Natl. Acad. Sci. USA* **100**, 3351–3356.

[12] Alter, O. & Golub, G. H. (2004) *Proc. Natl. Acad. Sci. USA* **101**, 16577–16582.

[13] Golub, G. H. & Van Loan, C. F. (1996) *Matrix Computation*, (Johns Hopkins Univ. Press, Baltimore) 3rd Ed.

[14] De Lathauwer, L., De Moor, B. & Vandewalle, J. (2000) *SIAM J. Matrix Anal. Appl.* **21**, 1253–1278.

[15] Kolda, T. G. (2001) *SIAM J. Matrix Anal. Appl.* **23**, 243–255.

[16] Zhang, T. & Golub, G. H. (2000) *SIAM J. Matrix Anal. Appl.* **23**, 534–550.

[17] Tavazoie, S., Hughes, J. D., Campbell, M. J., Cho, R. J. & Church, G. M. (1999) *Nat. Genet.* **22**, 281–285.

[18] Kim, H., Golub, G. H. & Park, H. (2005) *Bioinformatics* **21**, 187–198.

[19] Caro, L. H., Smits, G. J., van Egmond, P., Chapman, J. W. & Klis, F. M. (1998) *FEMS Microbiol. Lett.* **161**, 345–349.

[20] Stuart, J. M., Segal, E., Koller, D & Kim, S. K. (2003) *Science* **302**, 249–255.

[21] Bergmann, S., Ihmels, J. & Barkai, N. (2004) *PLoS Biol.* **2**, E9.